Prediction study of structural, electronic and optical properties of $4C_{16}H_{10}Br_2O_2$ Bis (m-bromobenzoyl) methane crystals

R. Boudissa [a], Z. Zerrougui [b], M.A. Ghebouli [a], K. Bouferrache [c], L. Krache [d], T. Chihi [a], B. Ghebouli [e], Mohamed A. Habila [f], M. Fatmi [a,*], Mika Sillanpää [g]

[a] Research Unit on Emerging Materials (RUEM), University Ferhat Abbas of Setif 1, Setif, 19000, Algeria
[b] Laboratory of Studies Surfaces and Interfaces of Solids Materials, Faculty of Technology, University Ferhat Abbas of Setif 1, Setif, 19000, Algeria
[c] Department of Physics, Faculty of Sciences, University of Mohamed Boudiaf, M'sila, 28000, Algeria
[d] PQSD Laboratory, Department of Physics, Faculty of Science, University Ferhat Abbas of Setif 1, Setif, 19000, Algeria
[e] Laboratory for the Study of Surfaces and Interfaces of Solid Materials (LESIMS), University Ferhat Abbas of Setif 1, Setif, 19000, Algeria
[f] Department of Chemistry, College of Science, King Saud University, P.O. Box 2455, Riyadh, 11451, Saudi Arabia
[g] Department of Biological and Chemical Engineering, Aarhus University, Norrebrogade 44, 8000, Aarhus C, Denmark

ARTICLE INFO

ABSTRACT

By first-principles calculations with density functional theory and a pseudopotential approach, the structural, electronic, and optical properties of the anhydrous $4C_{16}H_{10}Br_2O_2$ Bis (2-Bromobenzoyl) Methane crystals in *Pbnc* (N°60) and $P2_1/c$ (N°14) space group are investigated. All computations are determined by a generalized gradient approximation, local density approximation and an ultra-soft pseudopotential. The calculated equilibrium parameters are in good agreement with their available experimental data. This calculation shows that the GGA/PW91 functional overestimate the lattice constant, unlike the LDA/CA-PZ. The Br–C bond distance of 1.856 (1.902) Å is comparable with experimental value of 1.901 (1.896) Å in *Pbnc* ($P2_1/c$) space groups. The direct band gap nature is obtained for both space groups *Pbnc* and $P2_1/c$, since the maximum of the valence band and the minimum of the conduction band are both situated at the YA center.

1. Introduction

The human body is made up of four elements, oxygen, carbon, hydrogen and nitrogen, having 96 % of the total mass. Heavy metal cations are in the form of traces and do not exceed 0.1 %. Metal ions have a fundamental role in the specific functions associated with biological processes in living things. The existence of traces of basic addition elements in a pure metal improves the physical characteristics of such material. Intermolecular interactions that are inherently weak compared to covalent or intramolecular bonds make it possible to distinguish between molecules and assemblies of molecules, often declared under the name "non-covalent interactions or weak interactions". These interactions do not modify the nature of the molecular species and influence the mode of assembly. Among the non-covalent interactions cited are those of van der Waals and bonds of the hydrogen type. The crystal structure of the compound $4C_{16}H_{10}Br_2O_2$ Bis (m-Bromobenzoyl) Methane can be found in three different space groups. E. Donald et al. [1] specified that the crystal structure shows a

Pnca (#60) space group. $C_{16}H_{10}Br_2O_2$ is a pale white crystalline solid, which is stored cold at −20 °C, and is included in the preparation of Furamidine (F863600) as an antimicrobial and antiparasitic agent, and having a melting point of 192–194 °C. Dominique et al. [2] synthesize the crystal structure of $C_{16}H_{10}Br_2O_2$ Bis(m-Bromobenzoyl) Methane and conclude that this structure is similar to $C_{16}H_{10}Cl_2O_2$, takes the space group $P21/c$ (#14), and has a molecular weight of 394.07. Liu et al. [3] summarizes various preparation strategies and synthesis mechanisms for COMs (Covalent Organic Frameworks (COFs)), electrochemical and synthesis and briefly describes advanced characterization techniques of COMs. Furthermore, the application of COM for removal of heavy metals, separation of dyes, purification of radionuclides, detection of pollutants etc, seawater desalination is described and discussed. Finally, perspectives on future design opportunities of COMs in water purification were proposed. Fang et al. [4] synthesis, biocharbon (biochar) and biocharbon-based materials in the removal of environmental pollutants, hydrogen production and carbon dioxide capture were summarized and compared. Shoji et al. [5] studied the compound $C_{26}H_{18}Br_2O_4$, and

concluded that the dihedral angle between the two benzene rings is 50.92 (14)° and a weak intermolecular C–H···O hydrogen bond exists between the methyl group and the carbonyl O atom. Gordon et al. [6] studied The Crystal Structure of Bis-(*m*-chlorobenzoyl)-methane by three anisotropic least squares refinement and concluded that the structure confirms conclusions from the structure of bis (m-Bromo-benzoyl) methane where the symmetry of the molecule was forced by the crystal symmetry. The crystals suitable for X-ray analysis of bis (m-bromobenzoyl) methane was prepared by the reaction of m-bro-moacetophenone with ethyl m-bromobenzoate in the presence of sodium amide [7] photographs indicated the unique Pnca space group, with network constants a = 26.48, b = 4.054, c = 12.79 A. The calculated density was 1.85 g/cm^3 for four molecules in the unit cell. In the present work, periodic DFT calculations were carried out to study the crystal structure and structural, electronic and optical properties of $C_{16}H_{10}Br_2O_2$ Bis(m-Bromobenzoyl) Methane in orthorhombic and monoclinic structure. We implemented two separate exchange-correlation functional GGA and LDA throughout the calculations. To our knowledge, no similar study of the compound $C_{16}H_{10}Br_2O_2$ Bis(m-Bromobenzoyl) Methane has been reported previously. Our future

(a)

(b)
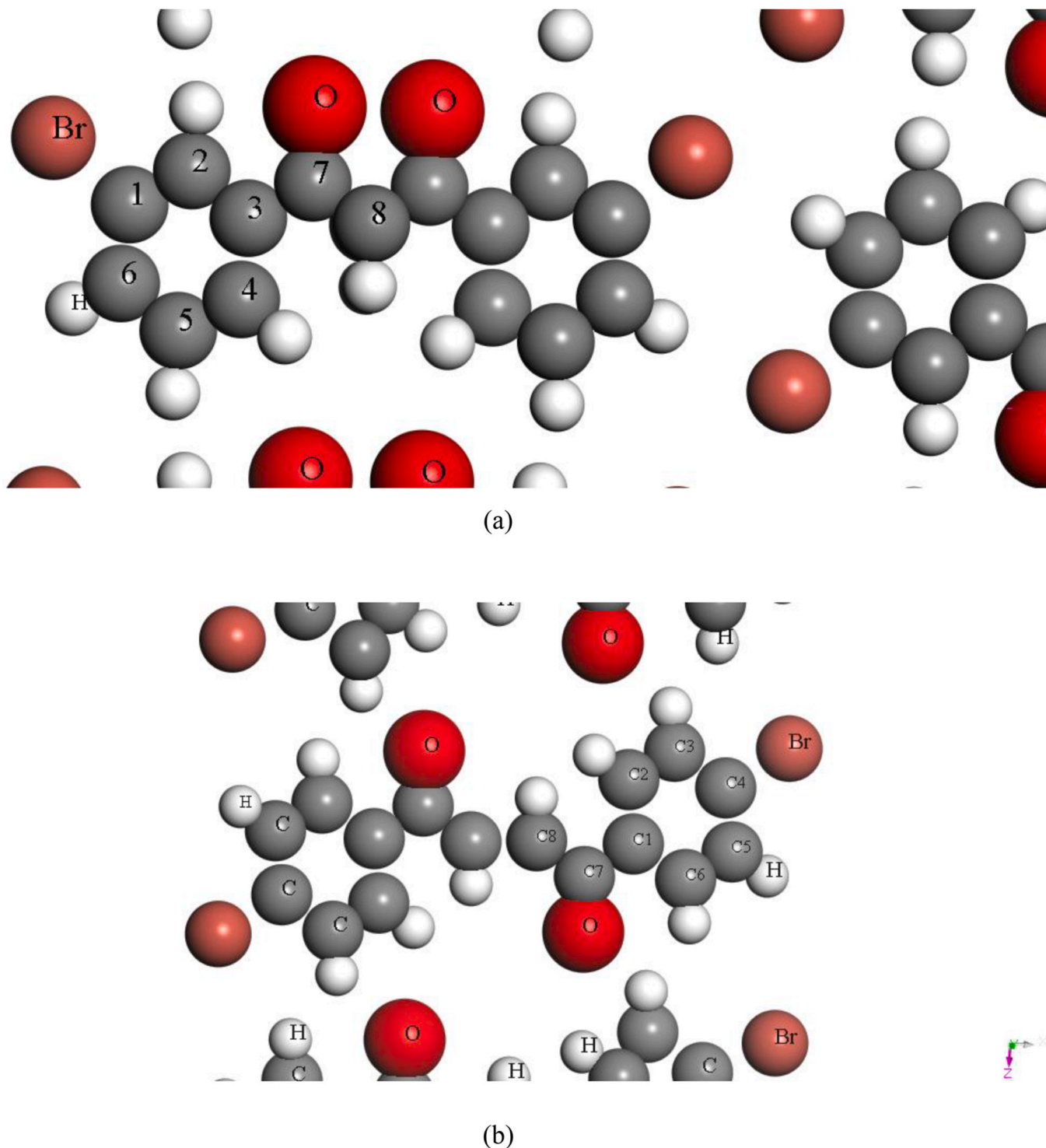
Fig. 1. The perspective view of $C_{16}H_{10}Br_2O_2$ in orthorhombic P*bnc* (N°60) (a) and monoclinic *P2$_1$/c* (N°14) (b) crystal structures.

objective is to study some compounds with other stoichiometric as $C_{13}H_9BrO$ and see their behavior with respect to $C_{16}H_{10}Br_2O_2$, and we hope this work will stimulate further experimental efforts to unveil the rich role of the structural, electronic and optic properties of bio-molecules systems in the solid-state toxic.

2. Computational details

Determining the ground state of a system is an important goal for theoretical chemistry. Indeed, many observable physical properties can be deduced from the ground state wave function. The density functional theory (DFT)-based first-principles plane-wave pseudo-potential approach was called CASTEP [8,9]. The Plane Wavelet Group developed the crystal wave functions with periodic boundary conditions and generalized gradient approximation for the exchange-correlation potential. The convergence of computed total energies with regard to the plane wave cut-off energy in the orthorhombic and monoclinic solid phases of the two molecular systems, which is determined to be 300 eV for orthorhombic Pnca (N°60), must first be investigated and examined. $P2_1/c$ monoclinic (N°14) and Z = 2 as shown in Fig. 1 (a and b) without taking account the spin polarized. The homogeneous electronic gas model served as the foundation for the LDA technique [10]. The electrical arrangement of H's valence: $1s^1$, C: $2s^2\,2p^2$, O: $2s^2\,2p^4$ and Br: $4s^2\,4p^5$. The basis set cut-off energy is set to 300 eV, and the Monkhorst-Pack grid is set to $1 \times 1 \times 1$ for the Brillouin zone [11]. The $C_{16}H_{10}Br_2O_2$ structure has been improved by using GGA/PW91 (Ganeralised Gradien Approximation, Perdew–Wang) and LDA/CA-PZ (local-density approximation, Ceperley−Alder, Perdew and Zunger) calculation to achieve a low total energy [12–14]. We find a configuration of atoms in space where the interatomic force on each atom goes to zero for a stationary position, which is stress minimization by definition in optimization geometry. It was achieved using self-consistency calculations with a tolerance of energy E = 2.10^{-5} eV/atom. Additional convergence thresholds, the total energy variation must be less than 2.10-6 eV/atom, the maximum force per atom must be less than 0.05 eV/A, the maximum stress must be less than 0.1 GPa, the maximum atomic displacement must be less than 0.002 A, and the maximum cycles must be less than 100. These parameters have also been adopted along the subsequent self-stability steps. To increase the accuracy of the calculations, the number of points is increased, but this increases the computational cost. After the geometry was optimized, the structure of the Kohn-Sham electronic domain and the partial density of state (PDOS) for each atom of the compound $C_{16}H_{10}Br_2O_2$ along the high-symmetry points of the Brillouin zone were investigated. references [15,16] provide a study of theoretical optical properties for light polarized along the [0 0 1] direction. Additionally, the electrical and optical properties of the $C_{16}H_{10}Br_2O_2$ crystal have been separately collected for GGA/PW91 and LDA/CA-PZ utilizing a cutoff energy and k-points of 300 eV.

3. Results and discussions

3.1. Structural properties

The crystal structures of $C_{16}H_{10}Br_2O_2$ are orthorhombic and monoclinic with space group Pnca N°. 60 and $P2_1/c$ N°. 14, where a typical cell consists of 120 atoms.

In Table 1, the calculated atomic coordinates for $C_{16}H_{10}Br_2O_2$ are reported and contrasted with the available experimental data [1]. According to the findings, the LDA/CA-PZ calculation and the available experimental ones agree to an acceptable degree. The effects of LDA/CA-PZ, Ecut = 300 eV, and k-meshes $3 \times 3 \times 3$ are described in Table 2 on the lattice parameters a, b, c, c/a and c/b ratios, volume cell, atomic number, density, and energy for both orthorhombic and monoclinic crystal structures of $C_{16}H_{10}Br_2O_2$. The LDA/CA-PZ provides reduced relative uncertainty for the lattice parameters in the ranges of

0.6 %–4.9 % and 0.4 %–3.05 %, followed by GGA/PBE in the ranges of 4.4 %–10.3 % and 0.7 %–16.9 % for orthorhombic and monoclinic crystal structure. Every LDA/CA-PZ parameter is getting closer to its experimental value. The LDA/CA-PZ, give the more stable $C_{16}H_{10}Br_2O_2$ molecule with minimum cohesive energy - 16963.594 eV and −8493.448 eV, while the minimum GGA/PBE cohesive energy is −16942.807 eV and −8482.981 eV for orthorhombic and monoclinic crystal structure. The calculated c/a and c/b ratios for LDA/CA-PZ are

Table 1
The atomic coordinates of $C_{16}H_{10}Br_2O_2$ in orthorhombic *Pnca* (N°60) and monoclinic $P2_1/c$ (N° 14) structures compared with the experimental values [1] (in parentheses).

Specie	X	Y	z
H	0.1352 (0.1308)-0.3870 (0.3772)	0.5911 (0.574) -0.3871 (0.4005)	0.1871 (0.2007)-0.6663 (0.6604)
H	0.1935 (0.1945) -0.2596 (0.2585)	0.7582 (0.749)-0.6501 (0.6460)	0.8887 (0.8962) -0.7453 (0.7375)
H	0.1205 (0.1212) −0.0870 (0.0970)	0.4875 (0.471) −0.6703 (0.6572)	0.8242 (0.8163) −0.4530 (0.4553)
H	0.0521 (0.0524) −0.2199 (0.2174)	0.2445 (0.245) −0.4167 (0.4236)	0.9269 (0.9262) −0.3706 (0.3781)
H	0.2408 (0.2500) −0.4706 (0.4715)	0.0263 (0.000) −0.0870 (0.0818)	0.9678 (0.9676) −0.6056 (0.5953)
C	0.0890 (0.0883) −0.3119 (0.3105)	0.3964 (0.399) −0.3858 (0.3876)	0.0661 (0.0684) −0.5118 (0.5110)
C	0.1314 (0.1291) −0.3220 (0.3212)	0.5389 (0.553) −0.4494 (0.4543)	0.1069 (0.1166) −0.6172 (0.6188)
C	0.1704 (0.1678) −0.2503 (0.2503)	0.6548 (0.683) −0.5975 (0.5990)	0.0477 (0.0546) −0.6629 (0.6653)
C	0.1665 (0.1648) −0.1671 (0.1673)	0.6507 (0.651) −0.6729 (0.6726)	0.9434 (0.9450) −0.6028 (0.6034)
C	0.1237 (0.1234) −0.1543 (0.1538)	0.5033 (0.494) −0.6104 (0.6073)	0.9053 (0.9005) −0.4981 (0.4962)
C	0.0850 (0.0843) −0.2271 (0.2258)	0.3683 (0.366) −0.4696 (0.4666)	0.9634 (0.9618) −0.4532 (0.4507)
C	0.2069 (0.2101) −0.3870 (0.3859)	0.8501 (0.850) −0.2348 (2399)	0.1153 (0.1047) −0.4596 (0.4570)
C	0.2430 (0.2500) −0.4665 (0.4672)	0.0014 (0.000) −0.0791 (0.0760)	0.0504 (0.0520) −0.5219 (0.5218)
O	0.2012 (0.2097) −0.3819 (0.3816)	0.8637 (0.848) −0.2339 (0.2478)	0.2064 (0.2068) −0.3648 (0.3613)
Br	0.0379 (0.0360) −0.0682 (0.0690)	0.2516 (0.2306) −0.8626 (0.8634)	0.1520 (0.1554) −0.6665 (0.6683)

Table 2
The lattice parameters c/a, c/b ratios, volume, density, atomic number and energy of in P*bnc* (N°60) (a), P2$_1$/c (N°14) compound.

$C_{16}H_{10}Br_2O_2$	Experiment	LDA	GGA
Space group	Pbnc (Orthorhombic N°60) [1]- P2$_1$/c (Monoclinic N°14)	Pbnc (N°60)- P2$_1$/c (N°14)	Pbnc (N°60)- P2$_1$/c (N°14)
Lattice parameter (Å)	26.48–14.44	26.637–14.283	28.674–14.338
b (Å)	4.054–3.9937	3.855–4.0123	4.474–4.6715
c (Å)	12.79–12.7244	13.336–13.1124	14.222–13.7400
c/a	0.483–0.881	0.500–0.918	0.496–0.958
c/b	3.155–3.186	3.456–3.268	3.178–2.941
Cell volume (Å^3)	726.92	1369.842–746.343	1702.308–914.926
Z	2	4–2	4–2
Calculated density (gcm^{-3})	1.8–1.8	1.91075–1.75350	1.53757–1.43040
Number of atoms in cell	120–120	120–120	120–120
Energy (eV)		−16963.594→-8493.448	−16942.807→-8482.981
β	97.827	96.689	96.205

0.5 (0.918) and 3.456 (3.268), while for GGA/PBE they are 0.496 (0.958) and 3.178 (2.941) for orthorhombic (monoclinic) crystal structure. The values of (LDA/CAPZ) agree with the experimental data 0.483 (0.881) and 3.155 (3.186) for orthorhombic (monoclinic) crystal structure. We have adopted the LDA functional in all the calculations. The molecule $C_{16}H_{10}Br_2O_2$ is visualized in Fig. 1 in *Pnca* (N°60) and $P2_1/c$ (N° 14) space group, where the shortest distances are represented.

Brillouin zones are used to describe and analyze the energy of the electron in the energy band structure of crystals. To define lines in reciprocal space, giving the coordinates of the starting and ending points and the number of points for each line. The coordinates of the start and end points can be given explicitly with three real numbers. On the principal directions of BZ in reciprocal space Fig. 2, According to the reciprocal lattice unit vectors, the high symmetry lines connecting the following high symmetry points were used to construct the electronic band diagram: Γ(0; 0; 0); Z (0; 0; 0.5); T (-0.5; 0; 0.5); Y (-0.5; 0; 0); S (−0.5; 0.5; 0); X (0; 0.5; 0); U (0; 0.5; 0.5); R (-0.5; 0.5; 0.5).

3.2. Electronic proprieties

The energy bands give the possible energies of an electron as a function of the wave vector. These bands are therefore represented in reciprocal space, and to simplify; only higher directions symmetries in the first Brillouin zone are treated. The density of electronic states is defined as the number of electronic states accessible (occupied or unoccupied) by an electron in an energy interval. The total density of electronic states of a crystalline solid is generally expressed in the primitive cell of the lattice in (Number of states/Energy). The results of the electronic band structures of $C_{16}H_{10}Br_2O_2$ in *Pbnc* and $P2_1/c$ space group, using LDA/CA-PZ functional are shown in Fig. 3. The calculated band gap is 0.736 eV with direct G - G nature, while in *Pbnc* it is 2 eV and indirect YA – Z nature in ($P2_1/c$). The top of the valence band (VB) taken as reference 0 eV is assigned to the Fermi level E_F as can be seen in Fig. 4. The valence levels are formed by a set of continuous levels in particular along the line G-Z (G-Y and A-B) in *Pbnc* (P2_1/c) space group of the BZ, where this continuum forms a set of narrow sub-bands especially along the line U–R and E-C in *Pbnc* and $P2_1/c$ space group of the ZB. The similarity is observed in the two band structures reflecting a closer atomic distribution. We can distinguish some important valence region between −20 eV and 0 eV. The peak at −20 eV of O-s and a small contribution of C-s. The decomposition of the bonds indicates that the low-lying structure near −15 eV has a mixed character of C-s, Br-s, and
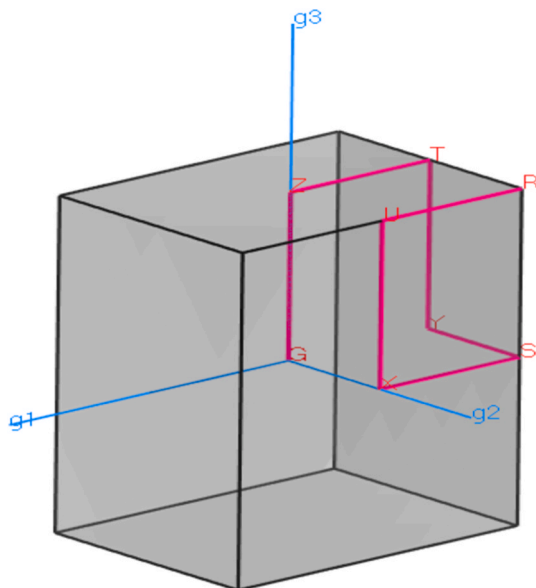

Fig. 2. The $C_{16}H_{10}Br_2O_2$ crystal structure in the unit cell and the BZ of this one.
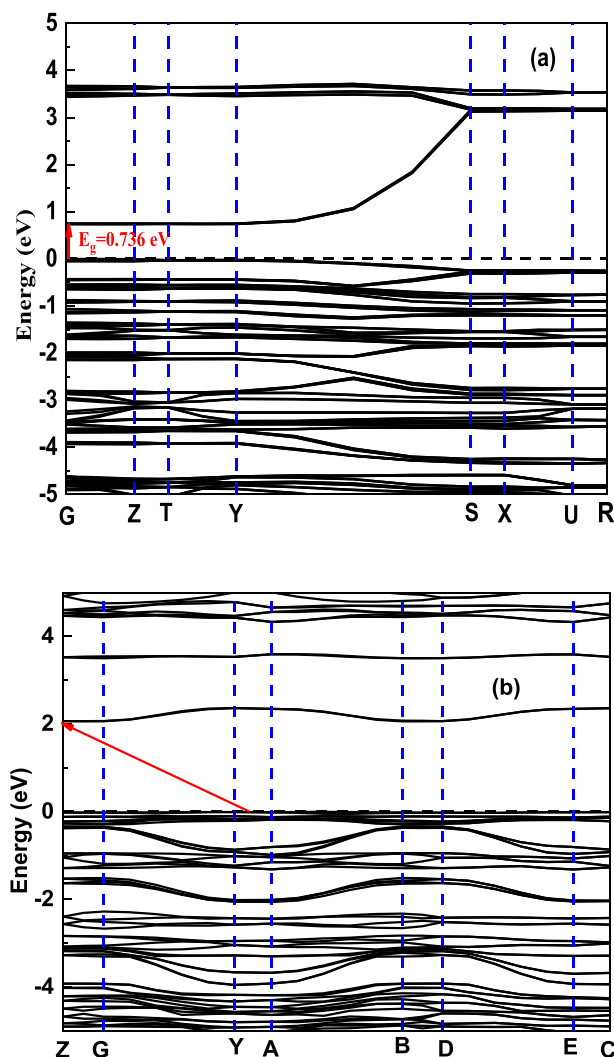

Fig. 3. DFT calculated Band structure of $C_{16}H_{10}Br_2O_2$ in P*bnc* (a), and P2_1/c (b) space group.

small contribution of C-p character. C-p, Br-p, O-p, and a minor amount of H-s character all contribute between −10 eV and the top of the valence band. The mixed character of C-p and O-p, as well as a minor contribution from the character O-p in Pbnc and the character Br-p in P21/c, dominate the electronic states of the narrow peak of the conduction bands. As is well knowledge, semiconductors with band gaps between 1.1 and 1.5 eV have the best chance of producing an effective solar cell. There is hybridization between O-p, C-p and Br-p, which explains their covalent bonding.

3.3. Optical properties

More study is required, and we are currently taking optical characteristics into consideration to help us understand its electronic structure. To do that, let's compute certain optical properties of $C_{16}H_{10}Br_2O_2$ in Pbnc and P21/c space groups while taking various photon energies into consideration. The dielectric function $\varepsilon(\omega) = \varepsilon_1(\omega) + i\varepsilon_2(\omega)$ describes the relationship between their real and imaginary parts for the incident light polarized along the direction [100]. The absorbance and polarization characteristics of the material are described by the fundamental optical parameters $\varepsilon_1(\omega)$ and $\varepsilon_2(\omega)$, which are plotted in Fig. 5. The momentum matrix between the occupied and unoccupied electronic states provided by Ref. [17] is used to determine the imaginary portion $\varepsilon_2(\omega)$ of the dielectric function:
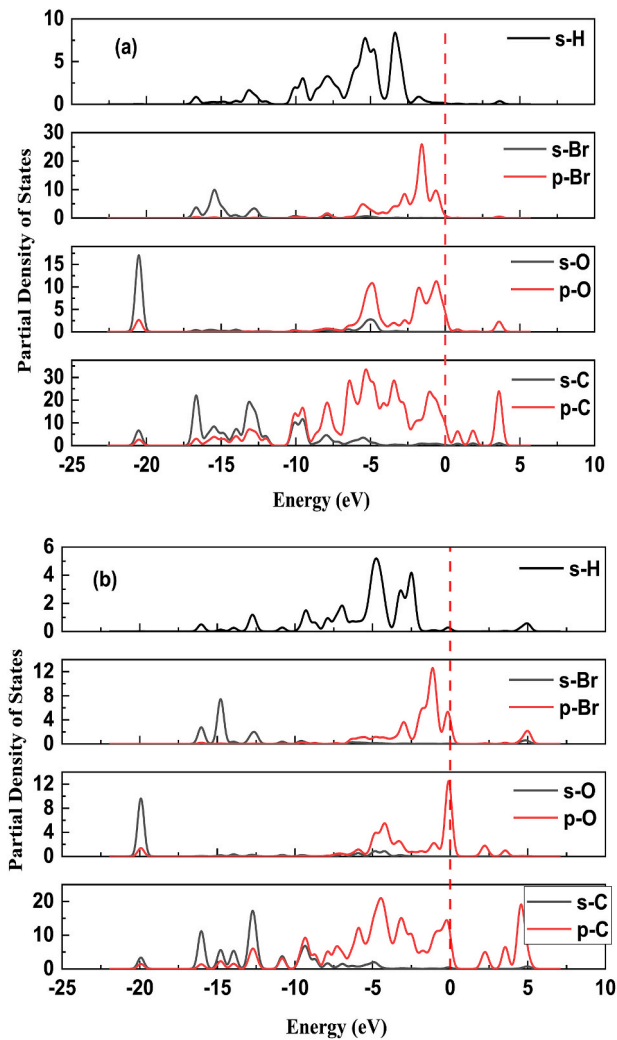
Fig. 4. The partial density of states of $C_{16}H_{10}Br_2O_2$ molecule in P*bnc* (a) and P2$_1$/c (b) space group.
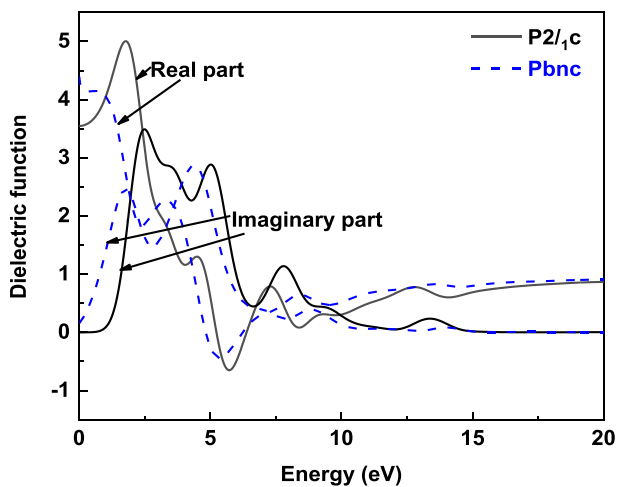

Fig. 5. Real and imaginary parts of the dielectric function of $C_{16}H_{10}Br_2O_2$ molecules in *Pbnc* and *P2$_1$/c* space groups as a function of energy.

$$\varepsilon_2(\omega) = \frac{2\omega^2\pi}{V\varepsilon_0} \sum_{k,\nu,c} |<\psi_k^c|\boldsymbol{u}.\boldsymbol{r}|\psi_\nu^c>|^2 \delta\left(E_k^c - E_k^\nu - \hbar\omega\right) \quad (1)$$

where **u** is the vector that determines how the incident electromagnetic radiation's electric field will be polarized, V is the volume of the unit cell and ψ_k^c represents the wave function of the valence (conduction) band at the wave vector k. However, using Kramers-Kronig relations [18], the real part of the dielectric function, ε_1 (ω), can be calculated from the imaginary part, ε_2 (ω).

$$\varepsilon_1(\omega) = 1 + \frac{2}{\pi}P\int_0^\infty \frac{\omega'\varepsilon_2(\omega')}{\omega'^2 - \omega^2} d\omega' \quad (2)$$

where P denotes the integral's primary value.

For the Pbnc and P21/c space groups, respectively, the dielectric constant ε_1 (0) was found to be 4.39 eV and 3.55 eV. When wavelengths are greater than 15 eV, ε_2 (ω) → 0, while ε_1 (∞) = 0.88 eV. The following equations can be used to get all additional optical properties, such as the refractive index $n(\omega)$, optical conductivity σ (ω), absorption coefficient α (ω), reflectivity $R(\omega)$, and loss function $L(\omega)$, Through ε_1 (ω) and ε_2 (ω) [19].

$$n(\omega) = \frac{1}{\sqrt{2}}\left[\sqrt{\epsilon_1^2(\omega) + \epsilon_2^2(\omega)} + \epsilon_1(\omega)\right]^{\frac{1}{2}} \quad (3)$$

$$\sigma(\omega) = \frac{\omega\varepsilon_2}{4\pi} \quad (4)$$

$$\alpha(\omega) = \sqrt{2}\omega\left[\sqrt{\epsilon_1^2(\omega) + \epsilon_2^2(\omega)} + \epsilon_1(\omega)\right]^{\frac{1}{2}} \quad (5)$$

$$R(\omega) = \left|\frac{\sqrt{\epsilon(\omega)}-1}{\sqrt{\epsilon(\omega)}+1}\right|^2 \quad (6)$$

$$L(\omega) = \frac{\epsilon_2(\omega)}{\epsilon_1^2(\omega) + \epsilon_2^2(\omega)} \quad (7)$$

The dimensionless quantity n (refractive index), describes the behavior of light in a medium; it depends on the measurement energy. Its plot is shown in Fig. 6. The static refractive index n (0) is 2.979 and 1.88 for *Pbnc* and *P2$_1$/c* space groups. The absorption coefficient, which also offers crucial information on the conversion of solar energy, indicates the region of the electromagnetic spectrum in which the material absorbs energy. For the Pbnc and P21/c space groups in the LDA method, Fig. 7 shows the optical absorption spectra of $C_{16}H_{10}Br_2O_2$ along the polarization direction [001]. Therefore, the obtained results
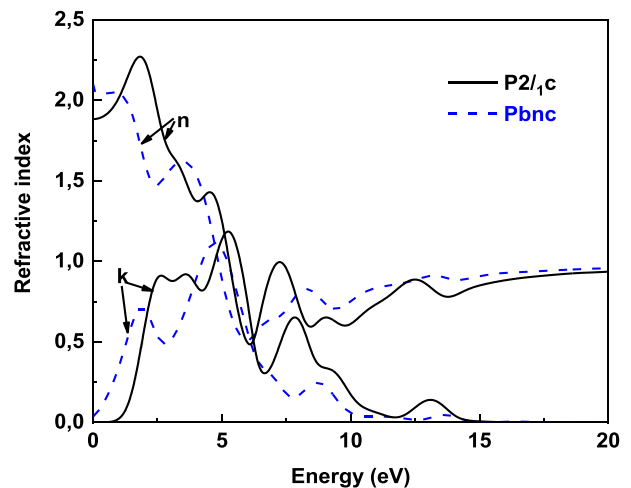

Fig. 6. The refractive index of $C_{16}H_{10}Br_2O_2$ in *Pbnc* and *P2$_1$/c* space groups as a function of energy.
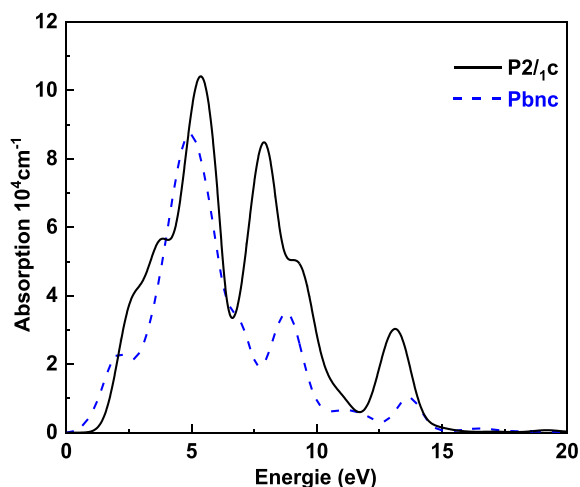
Fig. 7. The absorption of $C_{16}H_{10}Br_2O_2$ in *Pbnc* and *P2$_1$/c* space groups as a function of energy.

Fig. 9. The conductivity of $C_{16}H_{10}Br_2O_2$ in *Pbnc* and *P2$_1$/c* space groups as a function of energy.

indicate that $C_{16}H_{10}Br_2O_2$ crystal absorbs photon energy in the range 0.928 eV–15 eV and 0.342 eV–15 eV for the P*bnc* and *P2$_1$/c* space groups, *i.e.*, in the visible and ultraviolet region. Its absorption coefficient in the ultraviolet area is weak. The visible absorption spectra of the $C_{16}H_{10}Br_2O_2$ compounds in the P*bnc* (P2$_1$/c) space groups are shown in Fig. 7. It displays three absorption bands in the visible region (two strong and one weak) with absorption maxima at 8.72, 3.49, 1.02 and 10.41, 8.48, 3.03 respectively in the *Pbnc* and *P2$_1$/c* space groups.

At room temperature, the optical absorption coefficient of the compound $C_{16}H_{10}Br_2O_2$ in the P*bnc* (P2$_1$/c) space groups was determined in a spectral range from 0 to 15 eV. When electromagnetic waves penetrate a sample, if the penetration depth is lower the absorption coefficient is high [20]. For example, the values of AC near 5eV and 15eV are about 10.5×10^4 cm^{-1} and 0.2 $\times 10^4$ cm^{-1}, corresponds to the penetration depths of 0.10 μm and 5 μm, respectively. Fig. 8 show the reflectivity spectra as a function of photon energy. It starts at zero eV for the LDA functional. From this, it increases up to a maximum intensity of three maximums 1.44 eV–5.53 eV and 9.46 eV (2.33 eV–5.92 eV and 9.46eV) in the energy range of (0–15) eV for the *Pbnc* and *P2$_1$/c* space groups, it goes to zero at E = 15 eV. Fig. 9 show the conductivity of $C_{16}H_{10}Br_2O_2$ in *Pbnc* and *P2$_1$/c* space groups as a function of energy. It is through the absorption of electromagnetic radiation that the electrical conductivity of a given material increases. In our compound the real part of the optical conductivity starts with the photon energy ~ 1.035 (~ 0.36) eV for P2$_1$/c (*Pbnc*), as shown in Fig. 9. The electrical conductivity due to

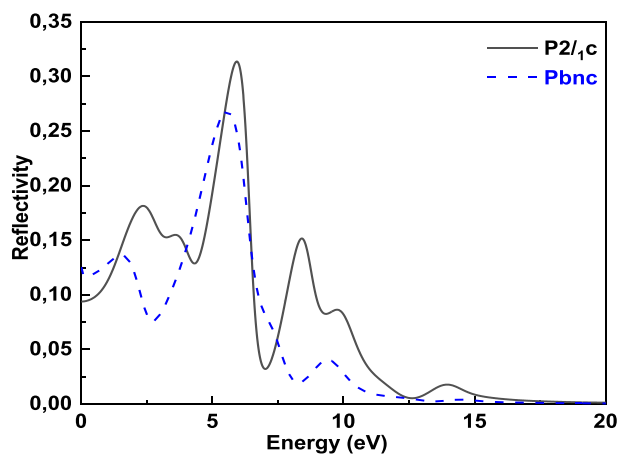absorption of Photon energy decreases in the energy range between 5 and 20 eV. The loss function represents many of the features of the imaginary part of the dielectric function. The loss function's information relates to the energy lost by an electron as it crosses a material [21]. It has to do with the plasma frequency ω_p, which happens when $\varepsilon_2 > 1$ and ε_1 approaches to zero. Fig. 10 presents a clear three-peak structure at energies between 0 and 15 eV. The energy loss function plotted for the *Pbnc* and *P2$_1$/c* space groups within LDA calculation considers the effective plasma frequency ω_p as 6.45 s^{-1} for both crystal structures.

3.4. Population analysis

Calculations of the Mulliken charges and bond populations using the formalism proposed by Segall et al. [22,23] demonstrate the electrostatic nature of this mechanism. A thorough examination of the solid-state structure of $C_{16}H_{10}Br_2O_2$ in the Pbnc and P21/c space groups reveals interactions between and among molecules that contain carbon centers. Table 3 and Table 4 summarize the obtained Mulliken charges for *Pbnc* and *P2$_1$/c* space groups for each atom of $C_{16}H_{10}Br_2O_2$ in the unit cell, with the carboxyl group having a charge of −0.30 e to 0.38 e (−0.06

Fig. 8. The reflectivity of $C_{16}H_{10}Br_2O_2$ in *Pbnc* and *P2$_1$/c* space groups as a function of energy.
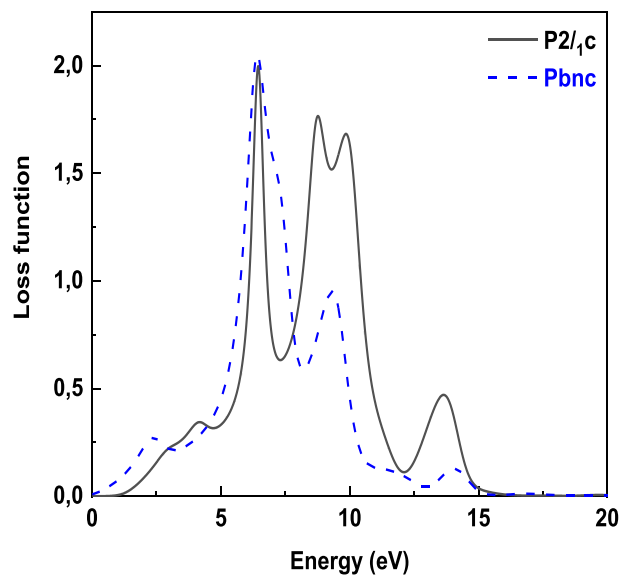

Fig. 10. The loss functions of $C_{16}H_{10}Br_2O_2$ in *Pbnc* and *P2$_1$/c* space groups as a function of energy.

Table 3

Mulliken of all electrons for $C_{16}H_{10}Br_2O_2$ in *Pbnc* (N°60).

Species	s-Orbitals	p-Orbitals	Total	Charge (e)
H	$0.70 \to 0.76$	0	$0.70 \to 0.76$	$0.24 \to 0.30$
C	$0.96 \to 1.29$	$2.67 \to 3.15$	$3.63 \to 4.44$	$-0.30 \to 0.38$
O	1.82	4.72	6.54	-0.54
Br	1.68	5.04	6.73	0.27

Table 4

Atomic populations (Mulliken) of all electron configurations of atoms for $C_{16}H_{10}Br_2O_2$ in *P2₁/c* (N°14).

Species	s-Orbitals	p-Orbitals	Total	Charge (e)
H	$0.68 \to 0.75$	0.00	$0.68 \to 0.75$	$0.25 \to 0.32$
C	$0.99 \to 1.17$	$2.62 \to 3.13$	$3.61 \to 4.30$	$-0.06 \to 0.39$
Br	1.83	4.71	6.54	-0.54
O	1.68	5.04	6.72	0.28

e to 0.39 e), the H group with 0.24 e to 0.30 e (0.25 e to 0.32 e), the Br group with 0.27 e (-0.54 e) and O: 0.54 e (0.28 e) in *Pbnc* and *P2₁/c* space groups. To understand Mulliken Population Analysis (MPA), the results show the interaction between the metal and the ligand as well as the various charge transfers that take place during redox processes. Carbon-carbon bond forming reactions played an enormously decisive and important role in shaping chemical synthesis of organic compounds. Table 5 and Table 6 for *Pbnc* and *P2₁/c* space groups summarize the electronic population in the different atomic, bonds, distances and the angles between the carbon atoms on one side, the carbon atoms and those of bromine on the other side, which are in good agreement with those given experimentally. It is also reported the weak Br–C, H–C, C–C, and O–C bonding in the two space groups with some discrepancies, Strong Br–H and O–H intermolecular contacts between pairs of $C_{16}H_{10}Br_2O_2$ diastereoisomers, as well as a few particularly strong connections, help pack the crystal of $C_{16}H_{10}Br_2O_2$.

4. Conclusion

Based on ab-initio calculations, we performed an extended study of the geometry optimization, electronic and optical properties for $4C_{16}H_{10}Br_2O_2$ Bis (*m*-Bromobenzoyl) Methane in *Pbnc* (N°60) and *P2₁/c* (N°14) space groups. We used the DFT- LDA/CA-PZ approach by means of the FLAPW method to calculate the physical properties. The equilibrium lattice parameters of $4C_{16}H_{10}Br_2O_2$ in *Pbnc* and *P2₁/c* space groups results in this study are more in line with published theoretical and experimental values. At room temperature, the optical absorption coefficient of the compound in $C_{16}H_{10}Br_2O_2$ was determined in a spectral range from 0 to 15 eV. When electromagnetic waves penetrate a sample, if the penetration depth is lower the absorption coefficient is high. The H group unit cell with 0.24 e to 0.30 e (0.25 e to 0.32 e), the Br group with 0.27e (-0.54 e) and O: 0.54 e (0.28 e) in *Pbnc* (*P2₁/c*) space groups. The $4C_{16}H_{10}Br_2O_2$ crystal absorb photonic energy in the ultraviolet range of 3.11–17.75 eV, making it a strong competitor as a coating material in this energy range. We looked at the impact of the GGA/PW91 and LDA/CA-PZ functionals on stability and lattice characteristics. The solid-state structure of $4C_{16}H_{10}Br_2O_2$ can be examined to reveal the interactions between and among carbon-containing molecules. The potent Br–H and O–H intermolecular interactions between pairs of $4C_{16}H_{10}Br_2O_2$ diastereoisomers. Mulliken population analysis reveals some significant Br–H and O–H intermolecular interactions, which aid in the packing of the $C_{16}H_{10}Br_2O_2$ crystal.

Funding

Table 5

Geometric parameters of $C_{16}H_{10}Br_2O_2$ in *Pbnc* (N°60) in brackets those given experimentally.

Bond	Population	Length (Å)
Br–C	$-0.36 \to 0.33$	1.856 (1.901)
H–C	$-0.25 \to 1.0$	$1.086 \to 2.948$
Br–H	-0.11	2.941
C–C	$-0.40 \to 1.16$	$1.368 \to 1.525$ ($1.375 \to 1.410$)
O–C	$-0.18 \to 0.14$	1.225 (1.306)
H–O	0.00	2.988
C2–C1–C6→119.5 (122.7)	C3–C4–C5→115.5 (119.6)	C6–C1–Br→122.2 (119.5)
C6–C1–C7→119.6 (118.7)	C4–C5–C6→124.3 (121.6)	O–C7–C3→121.8 (115.6)
C2–C3–C7→107.7 (119.3)	C5–C6–C1→117.8 (117.8)	O–C7–C8→119.4 (132.0)
C3–C2–C1→121.6 (119.1)	C3–C7–C8→105.9 (125.0)	
C4–C3–C2→120.7 (119.2)	C1–C2–Br→118.5 (117.8)	

Table 6

Geometric parameters (Å) of $C_{16}H_{10}Br_2O_2$ in *P2₁/c* (N°14) in brackets those given experimentally.

Bond	Population	Length (Å)
Br–C	$-0.36 \to 0.31$	1.902 (1.896)
H–C	$-0.16 \to 0.93$	1.092 → 2.778 (0.930)
Br–H	$-0.11 \to 0.08$	$2.934 \to 2.946$
C–C	$-0.27 \to 1.28$	$1.389 \to 1.520$ ($1.374 \to 1.492$)
O–C	$-0.20 \to 1.06$	1.237 (1.211)
H–O	$0.0 \to 0.01$	$2.435 \to 2.658$
C2–C1–C6→116.6 (118.3)	C3–C4–C5→122.9 (121.5)	C5–C4–Br→121.7 (119.37)
C2–C1–C7→123.7 (123.1)	C4–C5–C6→119.3 (118.8)	O–C7–C1→117.1 (121.0)
C6–C1–C7→119.6 (118.7)	C5–C6–C1→120.5 (121.3)	O–C7–C8→120.7 (119.7)
C3–C2–C1→123.6 (121.2)	C1–C7–C8→122.1 (119.3)	
C4–C3–C2→116.8 (119.0)	C3–C4–Br→115.3 (118.8)	

Declaration of competing interest

The author(s) declared no potential conflicts of interest with respect to the research, authorship, and/or publication of this article.

References

[1] D.E. Williams, Z.L. Dumke, R.E. Rundle, Acta Crystallogr. 15 (1962) 627.
[2] D.N. Lastovickova, J.J. La Scala, R.C. Sausa, Acta Crystallogr. E74 (2018) 352.
[3] X. Liu, Y. Li, Z. Chen, H. Yang, S. Wang, Z. Tang, X. Wang, Eco-Environment & Health 2 (2023) 117–130.
[4] Lin Fang, Tao Huang, Hua Lu, Xi-Lin Wu, Z. Chen, H. Yang, S. Wang, Z. Tang, Z. Li, B. Hu and X. Wang, 5 42 (2023).
[5] S. Watanabe, K. Nakaema, T. Muto, A. Okamoto, N. Yonezawa, Acta Crystallogr., Sect. A 66 2 (2010) 403.
[6] R. Gordon, R.E. Rundle, J. Am. Chem. Soc. 86 4 (1964) 574–581.
[7] W.G. Borduin, Substituent Effects on the Spectra and Ionization Constants of Diaroylmethanes, Unpublished M.S. thesis. Ames, Iowa, Library, Iowa State University of Science and Technology, 1954.
[8] Z. Zerrougui, M.A. Ghebouli, T. Chihi, S.I. Ahmed, L. Krache, B. Ghebouli, M. Fatmi, J. Mater. Res. Technol. 18 (2022) 396.
[9] J.P. Perdew, K. Burke, M. Ernzerhof, Phys. Rev. Lett. 77 (1996) 3865.
[10] J.S. Lin, A. Qteish, M.C. Payne, V. Heine, Phys. Rev. B 47 (1993) 4174.
[11] H.J. Monkhorst, J.D. Pack, Phys. Rev. B 13 (1976) 5188.
[12] P. Hohenberg, W. Kohn, Phys. Rev. B 136 (1964) 864.
[13] W. Kohn, L.J. Sham, Phys. Rev. 140 (1965) 1133.
[14] E.L. Albuquerque, U.L. Fulco, V.N. Freire, E.W.S. Caetano, M.L. Lyra, B.F. Moura, Phys. Rep. 535 (2014) 139.
[15] R.L. Araujo, M.S. Vasconcelos, C.A. Barboza, N.X. Lima, E.L. Albuquerque, U. L. Fulco, Comput. Theor. Chem. 1170 (2019) 112621.
[16] M. Jubair, A.M. Karim, M. Nuruzzaman, M.A. Zilani, J. Phys.Commun. 3 (2019), 055017.
[17] D. Li, F. Ling, Z. Zhu, X. Zhang, Phys. Rev. B Condens. Matter 406 (2011) 3299.
[18] Y. Fang, X. Kong, D. Wang, J. Lu, D. Cui, J. Phys. Chem. Solid. 127 (2019) 107.
[19] M. Zhong, Q.J. Liu, C.L. Jiang, F.S. Liu, B. Tang, X.J. Peng, J. Phys. Chem. Solid. 121 (2018) 139.
[20] I. Sharma, S. Reddy Madara, P. Sharma, Mater. Today Proc. 28 (2020) 402–407.
[21] M.A. Rahman, M.Z. Rahaman, M.A. Sarker, Comp. Condens. Matter. 9 (2016) 19.
[22] M.D. Segall, C.J. Pickard, R. Shah, M.C. Payne, Mol. Phys. 89 (1996) 571.
[23] M.D. Segall, R. Shah, C.J. Pickard, M.C. Payne, Phys. Rev. B 54 (1996), 16317.